Soft Matter

Accepted Manuscript

ROYAL SOCIETY OF CHEMISTRY

www.rsc.org/softmatter

Rings and Rackets from Single-Wall Carbon Nanotubes: Manifestations of Mesoscale Mechanics

Yuezhou Wang,[1] Matthew R. Semler,[2] Igor Ostanin,[3] Erik K. Hobbie,[2,4] and Traian Dumitrică[1,3,5,a)]

[1]*Department of Chemical Engineering and Materials Science, University of Minnesota, Twin Cities, MN, USA 55455*

[2]*Department of Physics, North Dakota State University, Fargo, ND, USA 55108*

[3]*Department of Civil Engineering, University of Minnesota, Twin Cities, Minnesota 55455, USA*

[4]*Department of Coatings and Polymeric Materials, North Dakota State University, Fargo, ND, USA 55108*

[5]*Department of Mechanical Engineering, University of Minnesota, Twin Cities, MN, USA 55455*

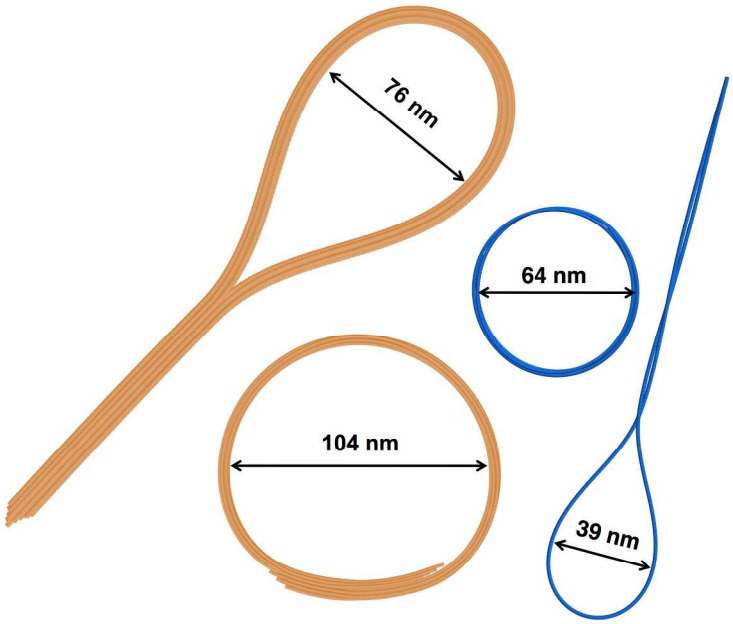

Abstract. We combine experiments and distinct element method simulations to understand the stability of rings and rackets formed by single-walled carbon nanotubes assembled into ropes. Bending remains a soft deformation mode in ropes because intra-rope sliding of the constituent nanotubes occurs with ease. Our simulations indicate that the formation of these aggregates can be attributed to the mesoscopic mechanics of entangled nanotubes and to the sliding at the contacts. Starting from the single-walled carbon nanotubes, the sizes of the rings and rackets' heads increase with the rope diameter, indicating that the stability of the experimental aggregates can be largely explained by the competition between bending and van der Waals adhesion energies. Our results and simulation method should be useful for understanding nanoscale fibers in general.

1. Introduction

Carbon nanotube (CNT) rings and rackets[1-4] are spontaneously-assembled fibrous aggregates that store significant bending deformations. While it is known that CNTs may contain defects that incur extended curvatures,[5] the observation that similar shapes exist in several fibrous biological materials[6,7] has prompted the hypothesis[8] that it is the slender fiber geometry - as opposed to molecular details related to particle composition - that lies at the origin of such shapes. It is thus important to investigate whether these CNT agglomerates can indeed be attributed to a competition between 'soft' bending modes and interparticle adhesion,[9,10] as the same questions will likely be encountered for other important filamentous assemblies, such as amyloid fibrils.[11] Because of their relatively simple and well-studied structure, CNTs represent an ideal system to investigate this hypothesis from a combined experimental and mesoscale modeling perspective, an approach that has not been previously pursued. Relying on recent progresses in CNT processing[12, 13] and mesoscale modeling,[14, 15] here we investigate a variety of ring and racket aggregate shapes assembled from length-purified single-wall carbon nanotubes (SWCNTs) and demonstrate the viability of such structures through direct mesoscale simulations focused on defect-free SWCNTs. The experimental-modeling comparison reveals the scaling of the sizes of the rings and rackets with the rope diameter, in agreement with the simple analytical modeling accounting of the bending strain and adhesion energies. The approach demonstrates the important role of mesoscopic mechanics in the formation of these agglomerates as well as the appeal of these morphologies for understanding the elastic and adhesion attributes of nanoscale fibers.

2. Results and Discussion

We first present some experimental results that demonstrate ring and racket formation in two different examples of purified SWCNTs. The ring structure shown in Fig. 1(a) was observed during the characterization of HiPCO SWCNTs that were purified through thermal oxidation at 260 ^{o}C, refluxing in HCl solution, and ultrasonication in nitric acid. Colloidal suspensions were then made from the purified SWCNT powder by sonicating the material in an aqueous solution of sodium dodecylbenzenesulfonate surfactant (SDBS, 0.6% by mass). After cold ultrasonication of the surfactant solution for 10 h, the nanotubes exist as 'ropes' or SWCNT bundles. Atomic-force microscopy (AFM) performed on dried films cast from dilute suspensions gave a mean bundle diameter of 13.5 nm and a mean length of 750 nm.[16] The AFM image shown in Fig. 1(a) was obtained by casting droplets of dilute SWCNT suspension on smooth silicon substrates and repeatedly wicking away excess isopropanol solution. Tapping-mode AFM measurements were performed in air using a Nanoscope IV AFM (Digital Instruments) operated under ambient conditions with 1-10 Ohm/cm phosphorus-doped silicon tips (Veeco; RTESP5, 125 μm length; 30 μm width, normal spring constant, 40 N/m; resonance frequency, 240 kHz to 300 kHz).

For the knot and racket images shown in Fig. 1(b)-(d), CoMoCat SWCNTs were dispersed in water via ultrasonication with 2% sodium deoxycholate (DOC) surfactant, coarsely centrifuged to remove impurities and bundles, and then purified by length using transient density-gradient ultracentrifugation in aqueous iodixanol solutions.[12, 13] The fraction of interest here was dispersed to the level of individual SWCNTs with mean length of order 700 nm and mean diameter of order 1 nm.[12, 13] For AFM characterization,

silicon wafers were functionalized with 3-(ethoxydimethylsilyl)-propylamine (APDMES, Sigma-Aldrich) by cleaning in a UVO chamber for 15 min followed by immersion into 1% APDMES in isopropanol for 20 min and subsequent rinsing with isopropanol and DI water. The wafers were dried in an oven at 70 ^{o}C for 20 min. SWCNT samples in 10 g/L DOC were diluted at least 100× with an aqueous solution of 0.2 wt. % sodium cholate and 20 mM sodium thiocyanate and deposited on a wafer by casting (5 to 20) μL of the sample, followed by incubation in a closed container for 8 min. After incubation, samples were blown dry using canned nitrogen. AFM imaging was done on a Bruker Dimension Icon AFM in the peakforce tapping mode (ScanAsyst) using ScanAsyst-Air probes.[17]

Figure 1. (a) A ring (diameter = 250 nm, height = 15 nm) spontaneously formed in a dried suspension of SWCNT ropes (scale bar = 50 nm). (b)-(c) Knots and rackets formed during the deposition of length-enriched suspensions of individual SWCNTs (scale bar =100 nm). The height legend for panels (b)-(d) is shown at the right. All shown structures are located on silicon wafer substrates.

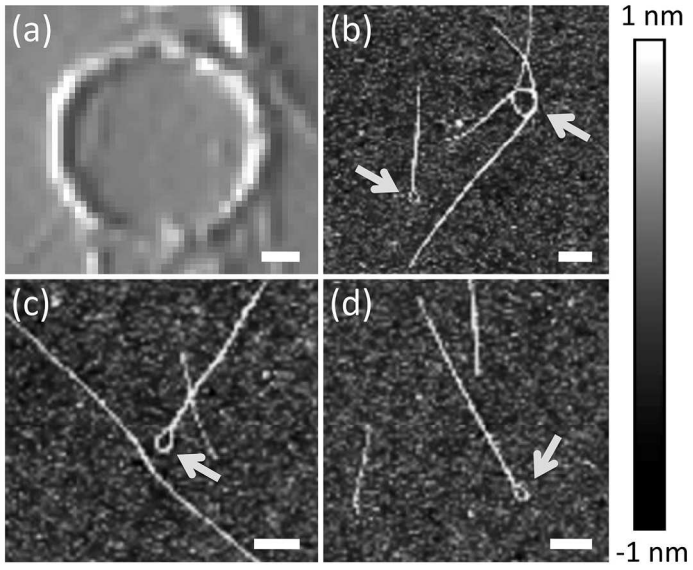

While the image in Fig. 1(a) depicts ropes that are several nanotubes in diameter, those in Fig. 1(b)-(d) depict structures that are primarily comprised of individual SWCNTs of various diameters. Interestingly, both sets of images portray bent SWCNT segments with local curvatures that are much

larger than what would be expected based on accepted values of the SWCNT persistence length (10-100 μm). Although these structures are rare, they are more prevalent than one might guess. For the length enriched CoMoCat SWCNTs shown in Fig. 1(b)-(d), for example, an ensemble of such AFM images suggests slightly less than a 2% probability for the formation of rings and rackets. One possible explanation for this seemingly anomalous degree of bending is that it represents a signature of the strength of attractive longitudinal van der Waals (vdW) forces between nanotubes. Testing this particular hypothesis numerically is impractical with atomic-scale simulations[18] because comprehensive simulations of μm long SWCNTs at this level of detail remains computationally prohibitive. More recently, multiscale approaches have been developed,[19-21] including the distinct element method (DEM) for nanotubes.[14, 15] With these methods, it is now possible to simulate complex SWCNT assemblies[9, 22] and investigate morphologies and mechanics[23] that have so far received very little computational attention.

DEM, the macroscopic method introduced by Cundall and Strack[24] more than 30 years ago, is currently used for simulating the mechanical properties of geological materials and structures. The method is natural for CNTs, which have macroscopic persistence lengths and whose mechanics is not sensitive to temperature.[25] We have recently adapted DEM at the mesoscale[14, 15] to simulate SWCNTs. We represented each SWCNT by a chain of rigid cylindrical segments interacting with each other via contact models informed by simulations we performed at the atomistic scale.[26-28] These contact models capture the effects of both covalent (parallel contact bonds within each SWCNT) and dispersion (vdW contact bonds between SWCNTs and SWCNT ends) microscopic forces. Ref.[15] gives a detailed description of how these microscopic interactions are incorporated into contact models. There and elsewhere,[29, 30] we have demonstrated the robustness of this methodology for investigating the mechanics of a variety of SWCNT systems, including ropes and networks. In summary, our DEM for

CNTs is based on a genuine solid mechanics method, which is augmented with long-range vdW forces encapsulated into a carefully designed anisotropic vdW contact model. These are key ingredients for investigating if the ring and racket morphologies formed by SWCNT ropes with free ends are the results of mesoscale mechanics, as we insure both accurate mechanics of individual SWCNTs and smooth vdW sliding of parallel portions of deformed or undeformed SWCNTs.

To investigate the viability of rings and rackets, we have performed DEM simulations that consider defect-free (10,10) SWCNTs. With the PFC3D[31] implementation at hand, the distinct elements - each 1.35 nm in length representing about 220 carbon atoms - are evolved in time under the forces and moments dictated by the contact models, with a damped dynamics scheme based on a velocity Verlet algorithm for translations and a 4-th order Runge-Kutta approach for rotations.[32] Our goal is not thermodynamic integration but driving the system toward metastable or stable states.

We now present the simulation results. We first demonstrate the key features of our model in four-point bending simulations conducted on crystalline ropes containing 80 nm in length SWCNT. The basic setup is shown in Fig. 2(a). Two-end roller support was imposed by fixing the y coordinates of selected elements located at the two ends (A and D). The other degrees of freedom of these elements are free so that the constituent SWCNTs are allowed to slide against each other. The load is applied on the elements located at the cross sections B and C, which are symmetrically spaced around the loading span. The distance between B and C is L=26 nm. The magnitude of the applied load ranges from 0.032 nN to 0.48 nN. We monitor the bending process by measuring the difference in deflection, □, between the elements located at the symmetry center and those at B and C, and the bending energy stored in the parallel contacts located in the volume between B and C. The geometrical relation $□(1-\cos(□/2□))=□$ is used to compute the bending radius R.

Figure 2(b) demonstrates linear variations of the bending energy vs. the curvature squared. The

bending moduli extracted from these simulations are presented in the inset to Fig. 2(b) and in Table 1. As shown in the last column of Table 1, the bending of a rope containing n SWCNTs can be described by an anisotropic beam with $B=nB_0$, where B_0 is the bending stiffness of an individual SWCNT. The sliding of the tubes against one another,[33] correctly captured by our anisotropic vdW model, represents a well-known obstruction towards the use of SWCNTs as building blocks in composite materials and structures. This behavior contrasts with what would be obtained by employing the usual isotropic treatment of the vdW interactions between coarse-grained elements. The isotropic treatment leads to staggering-induced corrugation,[14, 15] an artifact that prevents sliding of individual SWCNTs within the bent rope.

Figure 2. (a) Set-up for four-point bending simulations conducted with DEM. The down arrows indicate the location of the applied forces. The displacement in the scale bar is in Å. (b) Bending energy versus curvature squared for SWCNT ropes of various diameters. The inset shows the variation of the bending modulus with rope diameter.

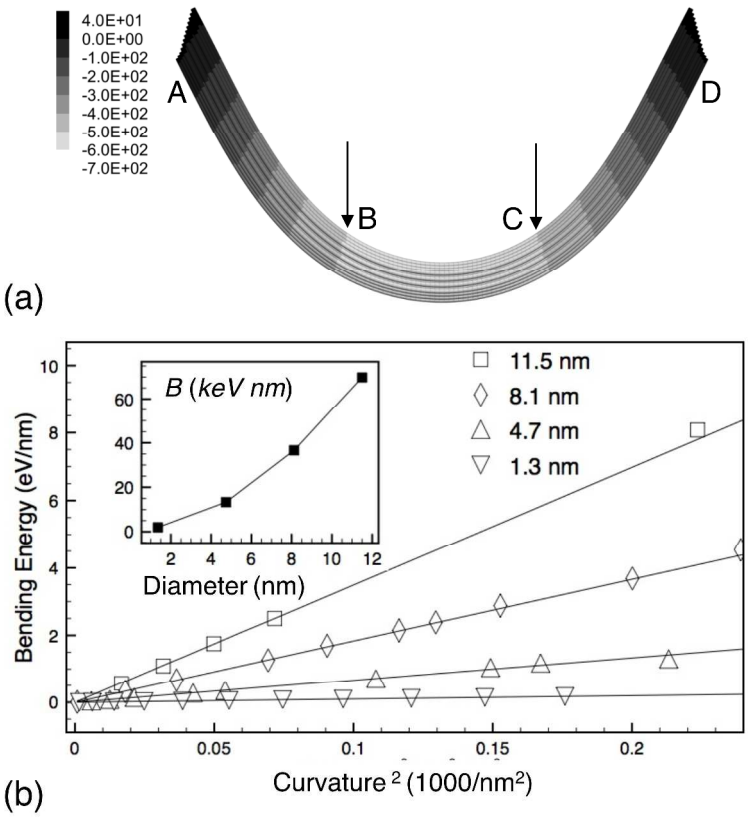

Figure 3. (a) Ring with one turn formed by a rope containing 7 SWCNTs each 400 nm in length. The inset illustrates the sliding of SWCNT rope at the free end. The final ring diameter is 104 nm. The overlap length *xL* is also shown. (b) A ring winding with three turns formed by a 540 nm long SWCNT. The final ring diameter is 64 nm. (c) Normalized total potential energy versus overlap for the two simulated ring morphologies, where the curves are predictions based on eq. (1) and Table 2. Parameter was set to -6.426 eV/nm for the rope-rope and to -2.114 eV/nm for the tube-tube interactions.[28] In deriving for rope-rope, we assumed a hexagonal close-packed rope structure and considered vdW tube-tube interactions up to the 3rd neighbor.

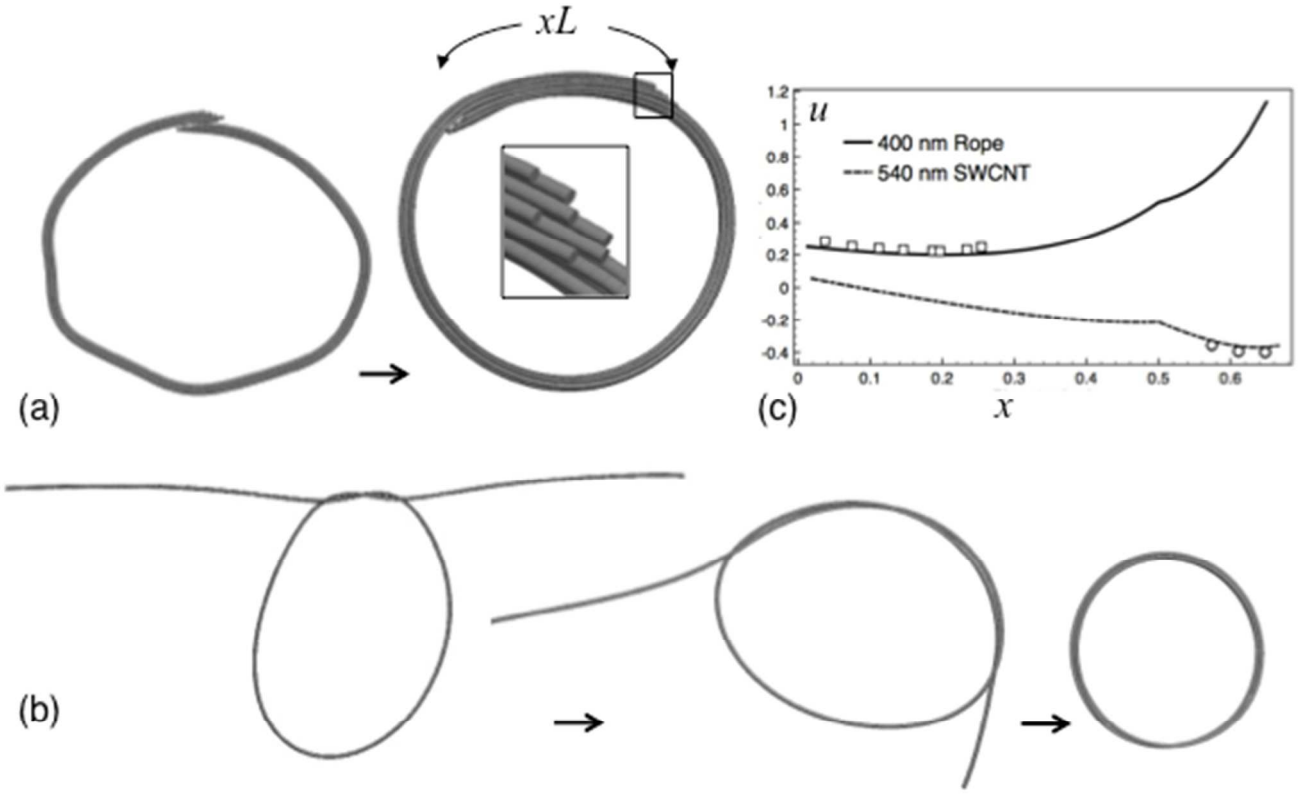

We now address the formation of ring-like aggregates. In Fig. 3(a) we consider the direct winding of an entangled rope. Starting from the zero-energy straight configuration, the rope was gradually bent so that the two ends are brought together into vdW contact [Fig. 3(a), left]. After some overlap was reached, the rope was relaxed and the two ends were stirred one past another. Stirring was necessary as the rope-rope sliding proved to be very slow. As shown in Fig. 3(c), stirring lowers of the total energy. The configuration shown in the right panel of Fig. 3(a) corresponds to the lowest energy point. It demonstrates that a SWCNT rope, such as the one shown in Fig. 1(a), can indeed be stabilized

by vdW adhesion. The sliding of the constituent SWCNTs visible in Fig. 3(a) ensures that bending of the rope is still a soft mode. Our DEM simulations beyond this state suggest that a further increase in overlap increases the total potential energy.

Table 1. Bending stiffness B as a function of the number of SWCNTs in the rope n. Results are obtained from four-point bending simulations conducted with DEM.

n	B (keV nm)	B/B_0
1	1.970	1
7	13.300	6.75
19	36.600	18.55
37	69.800	35.38

Table 2. Values for the dimensionless coefficients α and β describing the vdW adhesion. $\boldsymbol{x}$ is the normalized total overlap length[30] and n is the number of SWCNTs in the rope. Only rings with up to two turns are considered here.

x	n=1		n=7	
	α	β	α	β
(0,1/2)	0	1	0	1
(1/2,2/3)	-1.00474	3.009479	-1	3

In Fig. 3(b) we demonstrate the formation of a ring winding starting from a SWCNT initially entangled into a simple knot, such as the one shown in Fig. 1(b). Under relaxation, the radius of the central loop is increasing while the vdW forces and aligning moments are helping to attach the two free ends on the knot's central loop. The attachment of the two ends is followed by a sliding process, which results in a reduction of the ring radius. Thus, our DEM simulations demonstrate that knots with free ends, such as the one imaged in Fig. 1(b), are prone to form a ring winding. It is likely that the knot observed in experiment is stabilized by its contact with the other nanotube.

We find that a simple model comprising bending and adhesion energy components can explain the final equilibrium ring shapes. Let □ be the vdW adhesion energy per length between two ropes [Fig. 3(a)] or two SWCNTs [Fig. 3(b)] and let □ be the total overlap length, normalized by □. The total potential energy, in units of $|\zeta|L$, is[30]

$$\square = -\square - \square\square + 2\square^2\square/(1-\square)^2. \quad (1)$$

The linear term represents the vdW adhesion energy normalized by □□. In ring windings with multiple turns, this term is a piecewise function with the coefficients □ and □ given in Table 2. These coefficients were calculated analytically under the assumption that the nearest-neighbor distance between the overlapping turns corresponds to the 1.76 nm equilibrium intertube spacing between (10,10) SWCNTs[28] and that the parallel ropes ends do not coalesce into one to further lower the vdW energy. The last term represents the bending strain energy, where □ = □/□²|□|. Depending on the number of constituent SWCNTs, □ takes the values indicated in Table 1.

Fig. 3(c) plots the total potential energies predicted with eq. (1). The analytical approach shows that the 400 nm rope and the 540 nm SWCNT have only one minima corresponding to a single and a multiple (three) turn ring, respectively. The equilibrium DEM morphologies are located very close to the minima of the analytical curves. For the experimental longer and thicker rope, this analytical model also yields satisfactory prediction. For a rope with diameter 13.5 nm and length 750 nm, the stabilized configuration is predicted to be at radius of 116 nm with an overlap length of 20 nm. This is in good agreement with the experimental results shown in Fig 1 (a).

Figure 4. Racket morphology formed by (a) a 400 nm long rope containing SWCNT and (b) 460 nm (left) and 900 nm (right) SWCNTs. The lengths (widths) of the racket heads are 125 (76) nm, 77 (39) nm, and 70 (36) nm, respectively. (c) Total potential energy versus overlap the three simulated raket morphologies. The lines are predictions based on eq. (2) and Table 2.

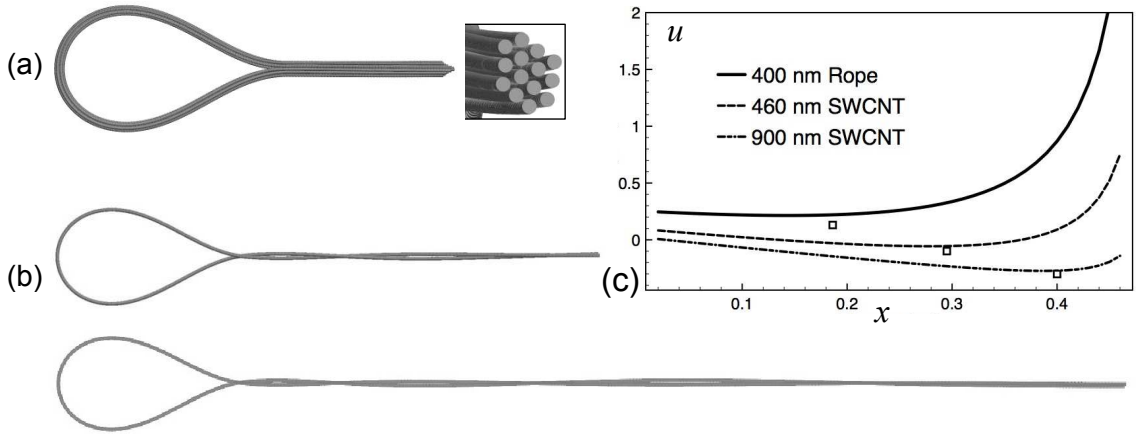

We have performed similar DEM simulations of racket agglomerates. The SWCNT rope was bent over onto itself, such that the inner sides of the two ends became parallel in vdW contact. Note that in the SWCNT case, it is not necessary that this entanglement be symmetric as the two ends are sliding past one another. Next, relaxation procedures were conducted, which produced the racket structures shown in Figs. 4 (a) and (b). The aggregates thus obtained closely resemble the ones indicated in the experimental images of Figs. 1(b)-(d) down to the scale of the racket head and the twisted structure of the handle.

Accounting for the competition between vdW adhesion and bending leads to[34]

$$\square = -\square + \square^2 b/(x - 0.5)\,. \qquad (2)$$

As can be seen from Fig. 4(c), the simulation data is located very close to the energy minima of the analytical curves. The lower energies obtained in computation can be explained by the new adhesion and elastic effects accounted for in the DEM simulations. Fig. 4(a) shows that under vdW forces, the two ends of the rope containing 7 SWCNTs spontaneously mix their structure to form a single rope. Note that the end of the handle is still a new surface formed by sliding effect, whose energy penalty is about 10% of the total potential energy. In rackets formed by SWCNTs, Fig. 4(b), the two ends form a helical handle. For the morphology shown in the top of Fig. 4(b), our analysis of the strain energy indicates that the onset of twisting reduces the total elastic strain energy by ~11 % while affecting the curvature and dimensions of the head. We also note that the racket dimensions are not changing significantly with the SWCNT length.

Having established the stability of the DEM simulated agglomerates, we now make an important connection with experiment. An important feature of both ring and racket configurations is the weak dependence of the aggregate dimensions on □. This dependence can be extracted by knowing the

minimal length to yield stable agglomerates,[14,34] which scales with $(B/\zeta)^{1/2}$. Accepting that □ ∝ □ and □ ∝ □$^{1/2}$, it follows that the radius of curvature scales as □$^{1/4}$.

The scaling derived above indicates that there should be an increase in the sizes of the rings and rackets' heads that is most noticeable in the very small rope diameter range. To test it, we have performed further experimentation to create and analyze aggregates of SWNCT ropes. We diluted a 1% DOC solution of the length-enriched CoMoCat SWCNTs described previously by a factor of 250:20 with purified DI water. Silicon wafer substrates were ultra-sonicated in acetone for 20 min, exposed to UVO plasma for 15 min, and then rinsed with DI water and dried under N_2 several times. The substrates were observed under 50×magnification to ensure cleanliness and then annealed in the SWCNT solution for 2 h before submerging them in an ethanol bath for 19 h to remove all DOC. The sample was then rinsed with ethanol and water several times and dried under N_2. To measure structure dimensions, AFM scans 20 μm × 20 μm in area were collected to identify surfactant-free regions with an appropriate density of nanotubes. When such areas were located, 5 μm × 5 μm scans were made at a scan rate of 3 lines per second. Measurements were made on a Veeco DI-3100 AFM in tapping mode using Golden Si NSG01 bare 10 nm probes. The in-plane shape dimensions of the observed rackets and rings are large enough to be easily resolved with the 10 nm probes, while the diameters of the constituent ropes were determined from height measurements, which have a much better resolution.

The analysis of the obtained aggregates is summarized in Fig. 5. One can see that indeed the agglomerate dimensions are increasing with increasing the rope diameter. The dependence of ring size on rope diameter is essentially linear and extrapolates to zero close to what corresponds to the mean minimum nanotube diameter in the ensemble (around 0.7-0.8 nm). The racket dimensions, in contrast, show percolative behavior, scaling roughly as $(d - d_c)^{\eta}$ with $\eta \approx 0.4$ for both the length and width of the racket heads. The measured aspect ratio of the rackets is always close to 2, independent of bundle

diameter. Interestingly, the threshold d_c = 0.78 nm is also close to the minimum diameter of an individual SWCNT. The region close to *dc* should be viewed as a step corresponding to the smallest equilibrium racket size for an individual SWCNT.

In scrutinizing our experimental data, we found that it was very important to limit our analysis to agglomerates that had minimal contact with other aggregates and bundles. Without this requirement, the measured trends shown in Fig. 5 were obscured, or even reversed, suggesting that entanglements with other aggregates can act to stabilize rings and rackets at much larger dimensions than would occur in isolation. This makes sense physically, since external perturbations arising from other structures will compete with those identified in the model and simulations.

Judging from the comparison with theory, we conjecture that most of the morphologies characterized in Fig. 5 are not far from the optimum balance between the elastic bending and rope-rope attraction. In Fig. 5(a) the measured diameter of the ring formed by a single SWCNT is in remarkable agreement with the predictions given by the model (1) and DEM simulations. The rings formed by the ~2.5 nm ropes appear, however, to be larger than what is predicted by the model, suggesting that these structures are not yet fully relaxed. Nevertheless, the predicted racket dimensions have similar magnitudes and increasing trends as the data in Fig. 5(b). Insights from the DEM simulations help clarify these differences. While in our simulations SWCNT-SWCNT sliding occurs with ease, the rope-rope vdW sliding is a slow process. While the ring morphology is directly impacted by the vdW sliding, the racket head dimensions are less sensitive to the degree of overlap achieved in the handle.

Figure 5. (a) Measured and computed ring diameter as a function of rope diameter with a linear fit. (b) Measured and computed racket head dimensions as a function of rope diameter with fits, as described in the text. Black markers are measured and gray (full and empty) markers are predicted by the models (1) and (2). The number of SWCNTs in the rope *n* is also shown.

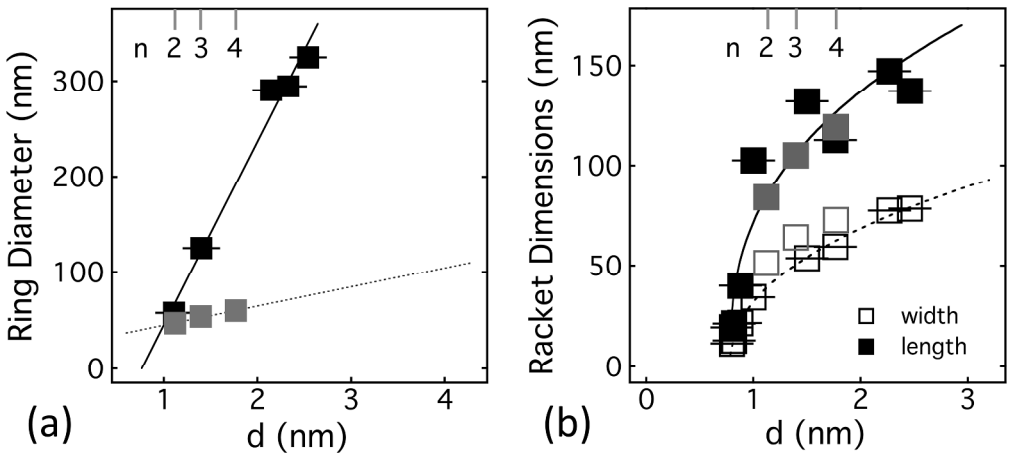

Conclusions

In summary, we report a variety of rings and rackets formed by CNTs synthesized and processed by two different methods. DEM simulations directly demonstrated the formation and stability of agglomerates composed of defect-free SWCNTs with realistic lengths. The remarkable agreement between experiment and theory supports the conclusion that the formation and stability of rings and rackets is the result of the interplay between the mesoscopic mechanics and adhesion attributes of SWCNTs. In particular, we foresee that the racket morphologies could be exploited for quantifying the elastic and adhesion attributes of other fibrous materials. The recently developed DEM mesoscale simulation approach should be also applicable to investigate agglomerates formed by other fibrous nanomaterials.

Acknowledgements

We thank Itasca Consulting Group for the PFC3D software support. Y. W., I.O, and T.D. acknowledge support of the NSF through CMMI 1332228. EKH and MRS acknowledge the support of the NSF through CMMI-0969155. We thank Jeffrey A. Fagan and Ming Zheng at NIST for providing the length-enriched CoMoCat SWCNTs and the images used in Fig. 1(c)-(d).

3. References

[a]Electronic mail: dtraian@umn.edu

1. R. Martel, H. Shea and P. Avouris, *Nature*, 1999, **398**, 299.
2. Q. Cao, M. G. Xia, M. Shim and J. A. Rogers, *Adv. Funct. Mat.*, 2006, **16**, 2355.
3. J. Liu, H. Dai, J. H. Hafner, D. T. Colbert, R. E. Smalley, S. J. Tans and C. Dekker, *Nature*, 1997, **385**, 780-781.
4. W. Wang, E. D. Laird, Y. Gogotsi and C. Y. Li, *Carbon*, 2012, **50**, 1769 –1775.
5. S. Ihara and S. Itoh, *Carbon*, 1995, **33**, 931.
6. D. K. Fygenson, J. F. Marko and A. Libchaber, *Phys. Rev. Lett.*, 1996, **79**, 4497.
7. D. DeRosier, L. Tilney and P. Flicker, *J. Mol. Biol.*, 1980, **137**, 375.
8. A. E. Cohen and L. Mahadevan, *Proc. Natl. Acad. Sci. U S A.*, 2003, **100**, 12141.
9. M. J. Buehler, *J. Mat. Res.*, 2006, **21**, 2855-2869.
10. Z. R. Abrams, Y. Lereah and Y. Hanein, *Nanotechnol.*, 2006, **17**, 4706-4712.
11. R. Paparcone, S. Cranford and M. J. Buehler, *Nanoscale* 2011, **3**, 1748.
12. J. A. Fagan, M. L.Becker, J. Chun, P. Nie, B. J.Bauer, J. R. Simpson, A. R. H. Walker and E. K. Hobbie, *Langmuir* 2008, **24**, 13880.
13. J. A. Fagan, M. Zheng, V. Rastogi, J. R. Simpson, C. Y. Khripin, C. A. S. Batista and A. R. H. Walker, *ACS Nano*, 2013, **7**, 3373.
14. T. Anderson, E. Akatyeva, I. Nikiforov, D. Potyondy, R. Ballarini and T. Dumitrică, *ASME J. Nanotech. Eng. and Med.* , 2010, **1**, 041009
15. I. Ostanin, R. Ballarini, D. Potyondy and T. Dumitrică, *J. Mech. Phys. Solids*, 2013, **61**, 762-782
16. D. Fry, B. Langhorst, H. Kim, E. Grulke, H. Wang and E. K. Hobbie, *Phys. Rev. Lett.*, 2005, **95**, 038304.
17. C. Y. Khripin, X. Tu, J. M. Heddleston, C. Silvera-Batista, A. R. H. Walker, J. Fagan and M. Zheng, *Anal. Chem.* , 2013, **85**, 1382.
18. S. Zou, D. Maspoch, Y. Wang, C. A. Mirkin and G. A. Schatz, *Nano Lett.*, 2007, **7**, 276-280.
19. M. Buehler, Y. Kong and H. Gao, *ASME J. Eng. Mater. Technol.*, 2004, **126**, 245–249.
20. L. Zhigilei, C. Wei and D. Srivastava, *Phys. Rev. B*, 2005, **71**, 165417.
21. A. N. Volkov and L. V. Zhigilei, *J. Phys. Chem. C*, 2010, **114**, 5513-5531.
22. A. N. Volkov and L. V. Zhigilei, *ACS Nano*, 2010, **4**, 6187-6195.
23. R. C. Picu, *Soft Matt.*, 2011, **7**, 6768-6785.
24. P. A. Cundall and O. D. L. Strack, *Geotechnique*, 1979, **29**, 47-65.
25. M. Xu, D. N. Futaba, T. Yamada, M. Yumura and K. Hata, *Science*, 2010, **330**, 1364.
26. I. Nikiforov, D.-B. Zhang, R. D. James and T. Dumitrică, *Appl. Phys. Lett.*, 2010, **96**, 123107.
27. D.-B. Zhang and T. Dumitrică, *Appl. Phys. Lett.* , 2008, **93**, 031919.
28. A. Carlson and T. Dumitrică, *Nanotechnol.*, 2007, **18**, 065706-065710.
29. I. Ostanin, R. Ballarini and T. Dumitrică, *J. Appl. Mech.*, 2014, **81**, 061004.
30. Y. Wang, C. Gaidau, I. Ostanin and T. Dumitrică, *Appl. Phys. Lett.*, 2013, **103**, 183902.
31. PFC3D (Particle Flow Code in 3 Dimensions), Version 4.0. Minneapolis: ICG Inc., 2008.
32. S. M. Johnson, J. R. Williams and B. K. Cook, *Int. J. Numer. Meth. Eng.*, 2008, **74**, 1303-1313.
33. J.-P. Salvetat, G. A. D. Briggs, J.-M. Bonard, R. R. Bacsa, A. J. Kulik, T. Stöckli, N. A. Burnham and L. Forró, *Phys. Rev. Lett.*, 1999, **82**, 944.
34. Two nonesential terms, which depend on the inter-rope spacing, have been omitted. For the complete model see: W. Zhou, Y. Huang, B. Liu, K. C. Hwang, J. M. Zuo, M. J. Buehler and H. Gao, *Appl. Phys. Lett.*, 2007, **90**, 073107.